CHAPTER V

Kuramoto-Sivashinsky system—(te:

$1-D$ KURAMOTO-SIVASHINSKY EQUATION AND ITS STEADY SOLUTIONS

The $1-d$ Kuramoto-Sivashinsky equation (KSe) is one of the simplest nonlinear PDEs that exhibit spatiotemporal chaos. As we will show, its asymptotic dynamics is equivalent to a finite set of ODEs, even in the chaotic regime. The study also helps us understand the phase dynamics of the CGLe discussed in chapter 4. In this chapter we discuss basic properties and the steady solutions of the KS equation. After deriving the KSe as a phase description of the CGLe in sect. 5.1, we present some of its properties under the periodic boundary condition in sect. 5.2. In sect. 5.3, we concentrate on the steady solutions of the KSe. In addition to reviewing others' work, we numerically determined the steady solutions most relevant to the phase space dynamics. They will be used in the calculation of periodic orbits in the next chapter.

5.1 Derivation

The KS equation is a generic equation that describes the evolution of the phase of coupled oscillating systems near the onset of spatial instability. Here we take the CGLe (70) as an example and derive the KSe near the onset of first spatial instability. Consider perturbations on the homogeneous oscillating state, *i.e.*, let $A(x,t)$ take the form

$$A(x,t) = (1+\rho(x,t))e^{i(-\beta t+\phi(x,t))} \,. \tag{124}$$

Substituting (124) into the CGLe (with $\mu = 1$), we get the exact evolution equation for $\rho(x,t)$ and $\phi(x,t)$,

$$\begin{aligned} \rho_t &= -2\rho - 3\rho^2 - \rho^3 + \rho_x - \alpha(1+\rho)\phi_{xx} - 2\alpha\rho_x\phi_x - (1+\rho)(\phi_x)^2 \,, \quad (125)\\ (1+\rho)\phi_t &= -2\beta\rho - 3\beta\rho^2 - \beta\rho^3 + \alpha\rho_{xx} + (1+\rho)\phi_{xx} \\ &\quad +2\rho_x\phi_x - \alpha(1+\rho)(\phi_x)^2 \,. \quad (126)\end{aligned}$$

For small perturbations, we only need to retain linear terms in (125), (126), and thus are able to use the Fourier modes to study the stability. Let

$$\begin{aligned} \rho(x,t) &= \rho_0 e^{i(\omega t - kx)} \\ \phi(x,t) &= \phi_0 e^{i(\omega t - kx)} \,, \end{aligned}$$

and by substituting them into the linear equations for ρ and ϕ, we get the relation

$$\begin{aligned} (i\omega + 2 + k^2)\rho_0 - \alpha k^2\phi_0 = 0 \\ (2\beta + \alpha k^2)\rho_0 + (i\omega + k^2)\phi_0 = 0 \,, \end{aligned} \tag{127}$$

which implies

$$i\omega = -(1+k^2) \pm \sqrt{1 - 2\alpha\beta k^2 - \alpha^2 k^4} \,.$$

One solution always has negative real part which is stable and the other solution may change the sign of the real part under system parameter changes. The latter one induces spatial instability and its dispersion relation for small k becomes

$$i\omega = -(1+\alpha\beta)k^2 - \frac{1}{2}\alpha^2(1+\beta^2)k^4 + O(k^6) \,, \tag{128}$$

which implies that the long wavelength modes become unstable first and evolve very slowly (at a time scale $1/t \sim (1+\alpha\beta)k^2$). To the lowest order, the phase thus satisfies a diffusion equation

$$\partial_t \phi = \nu \nabla^2 \phi \,, \tag{129}$$

with $D = 1 + \alpha\beta$. If $D > 0$ (the so-called Benjamin-Feir-Newell criterion), the phase will tend to be spatially uniform and the asymptotic state is the homogeneously oscillating state. If $D < 0$, (129) leads to unphysical blow-ups so higher order and nonlinear terms should be included to saturate the instability. Comparing the relative size of each term in (125) and (126) at the onset of instability, we find that in (125), -2ρ on the right hand side implies a fast decay of ρ and thus ρ is small and slaved to the gradient of ϕ. From (127), we see that

$$\frac{\rho_0}{\phi_0} \approx \frac{|\alpha|}{2}k^2 \,, \tag{130}$$

which shows $\rho_0 \to 0$ as $k \to 0$, as argued above. In view of (130) and (128), near the onset of spatial instability, the scalings are like

$$x \sim \epsilon \,,\ t \sim \epsilon^2 \,,\ \phi \sim 1 \,,\ \rho \sim \epsilon^2 \,.$$

Inserting into (127) and equating the terms of order ϵ^2, we get

$$\begin{aligned} 0 &= -2\rho - \alpha\phi_{xx} - (\phi_x)^2 \\ \phi_t &= -2\beta\rho + \phi_{xx} - \alpha(\phi_x)^2 \,, \end{aligned}$$

or

$$\phi_t = D\phi_{xx} + \lambda(\phi_x)^2 \,, \tag{131}$$

where $\lambda = \beta - \alpha$. Crossing the BFN instability, (131) becomes unstable and we have to retain higher order terms to stabilize it. The simplest choice is to include the fourth order term in (128) and we find that

$$\phi_t = D\phi_{xx} + \lambda(\phi_x)^2 - \mu\phi_{xxxx} \,, \tag{132}$$

where $\mu = \frac{1}{2}\beta^2(1+\alpha^2)$. To be consistent with the scaling relation, the fourth and the second order terms must have comparable size, which means $D \sim k^2$ and thus implies that (132) holds near the onset of instability and in the limit of large system size. In practice, (132) and its variants hold under less restrictive conditions and are able to describe the time evolution of a spatially extended system in quite large parameter range. In the following we are interested in the case where $D < 0$.

5.2 Basic Properties

The KS equation was initially derived as a phase equation by Kuramoto and Tsuzuki for a system of reaction-diffusion equations [155]. Sivashinsky derived it independently in the context of small perturbations of unstable flame fronts [232]. The equation also describes falling films on an inclined surface [233, 17], interfacial instability between two concurrent viscous fluids [128] and unstable drift waves in plasmas [39, 210]. By rescaling t, x and u in (132), we obtain

$$u_t = (u^2)_x - u_{xx} - \nu u_{xxxx}\,, \tag{133}$$

where ν is a viscosity-like parameter which controls the rate of dissipation in the system. The first term on the right of (133) is the nonlinear convection term which induces interaction between different Fourier modes. In average, it transfers energy from the low wavenumber modes to higher ones. The second term is an anti-diffusion term which pumps energy to the system and makes it unstable. The last term dissipates energy and stabilizes the system.

5.2.1 Symmetry and Fourier modes

Eq (133) is space and time translationally invariant. It also preserves antisymmetric solutions, *i.e.*, if $u(x,0) = -u(-x,0)$, then $u(x,t) = -u(-x,t)$ for any $t > 0$. It is Galilean invariant, *i.e.*, if $u(x,t)$ is a solution, then $c + u(x+2ct, t)$ with c an arbitrary constant, is also a solution.

We will study (133) in a periodic interval of size L. L will be used as the control parameter with ν fixed. In the literature the renormalized length $\tilde{L} = \frac{L}{2\pi\sqrt{\nu}}$ is also used as the bifurcation parameter. In view of the periodic boundary condition $u(x,t) = u(x+L,t)$, we expand $u(x,t)$ in Fourier modes,

$$u(x,t) = \sum_k a_k(t) e^{ikqx}\,, \tag{134}$$

where $a_k \in \mathbb{C}$ and $q = 2\pi/L$ is the basic wavenumber. The reality of u implies that $a_k^* = a_{-k}$. Eq (133) then takes the form

$$\dot{a_k} = [(kq)^2 - \nu(kq)^4]a_k + ikq \sum_{m=-\infty}^{\infty} a_{k-m}a_m\,, \tag{135}$$

where $\dot{a_k}$ denotes the time derivative of a_k. Note that $\dot{a_0} = 0$, so a_0 is a conserved quantity. By Galilean invariance, we may set $a_0 = 0$ without loss of generality. Note that in the subspace of antisymmetric solutions, the translational invariance of the original system reduces to the invariance of translation by half a period. In Fourier modes representation (135), it becomes an inversion invariance under $a_{2m} \to a_{2m}\,, a_{2m+1} \to -a_{2m+1}\,, m \in \mathbb{Z}$.

From (135), we see that the origin $u(x,t) \equiv 0$ has Fourier modes as the stability eigenvector and at most a finite of them are unstable. See in figure 13 how the linear eigenvalue depends on the wavenumber. Considering that this dependence is an even function of the wavenumber, we only show the positive part. It is easy to see that when $|kq| \in (0, 1/\sqrt{\nu})$, the corresponding Fourier modes are unstable. The most unstable modes has $|kq| = 1/\sqrt{2\nu}$

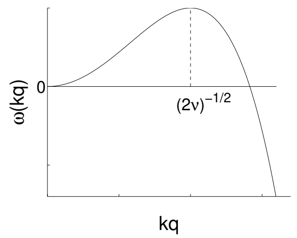

Figure 13: The stability eigenvalue of $u(x,t) \equiv 0$ versus the wavenumber kq.

and defines the scale of basic building blocks of the spatiotemporal dynamics of the KSe in large system size limit as shown later. In a periodic box, as the set of wavenumbers is discrete, finite gaps exist between different eigenvalues and the gap increases quickly with the increase of wavenumbers. Based on this special spectral structure, various properties of the KSe are derived [249].

5.2.2 Origin is the global attractor for small L

For L small enough, as shown above, all the Fourier modes become linearly stable so the origin is a local attractor. In fact, for $L < 2\pi\sqrt{\nu}$, we show that $u(x,t) = 0$ is also a global attractor. We denote the integral of a function A over $[0, L]$ by $\langle A \rangle$, *i.e.*,

$$\langle A \rangle = \int_0^L A(x,t)\,dx\,.$$

Multiplying both sides of (133) by $u(x,t)$ and then integrate, we have

$$\frac{1}{2}\langle u^2 \rangle_t = \frac{2}{3}\langle (u^3)_x \rangle - \langle u u_{xx} \rangle - \nu \langle u u_{xxxx} \rangle = \langle u_x^2 \rangle - \nu \langle u_{xx}^2 \rangle\,, \tag{136}$$

since $\langle (u^3)_x \rangle = 0$ due to the periodic boundary condition. For the same reason the partially integrated parts equal to zero. $\langle u \rangle_t$ means taking derivative with respect to time. Substitute (134) into the right hand side of (136), we get

$$\frac{1}{2}\langle u^2 \rangle_t = \sum_{k=-\infty}^{\infty} |a_k|^2 (kq)^2 (1 - \nu(kq)^2)\,. \tag{137}$$

It is easy to see that when $L < 2\pi\sqrt{\nu}$, each term on the right hand side of (137) is less than or equal to 0. So in this case, we conclude that

$$\langle u^2 \rangle_t \leq 0$$

$'='$ holds only for $u \equiv 0$. When $u \not\equiv 0$, $\langle u^2 \rangle_t < 0$, so $\langle u^2 \rangle$ keeps decreasing, the solution to (133) approaching $u(x,t) = 0$. So we have proved that the origin is a global attractor when $L < 2\pi\sqrt{\nu}$.

5.2.3 Inertial manifold

When L is large (or infinite), near the laminar solution $u(x,t)=0$, a band of Fourier modes with wave numbers $|kq| < 1/\sqrt{\nu}$ are unstable with the observed patterns dominated by the most unstable mode, with $|kq| = 1/\sqrt{2\nu}$. Away from $u=0$, the instability of these lower modes is balanced by the collective action of all the modes through the nonlinear convection term $(u^2)_x$, not like in the CGLe case where the stability is saturated by the nonlinear "diagonal terms" of the form $a_n \Sigma_k a_k^* a_k$ [41].

It has been shown that the solution $u(x,t)$ is analytic in x at any time $t>0$ if $u(x,0)$ is analytic, and thus the amplitudes of the high k modes decay at least exponentially [40]. In fact, an absorbing ball $\mathscr{B}$ exists such that all trajectories will be contained in it after a finite time interval depending on the initial conditions. The ω-limit set of $\mathscr{B}$ is thus the global attractor in the infinite-dimensional phase space of the KSe. The strong damping of the higher modes exerted by the super-viscosity term u_{xxxx} produces a finite-dimensional invariant manifold Σ which is compact and attracting. With these properties, it has been named *inertial manifold* [86, 87, 249]. All solutions converge exponentially to Σ and therefore Σ contains the global attractor. Σ acts like a global center manifold and a finite number of Fourier modes are enough to pin it down. The rest higher modes are contained in the geometrical constraints that define Σ [195]. Various numerical procedures have been proposed to approximate inertial manifolds [85].

Though the fractal dimension of the global attractor and the inertial manifold can be rigorously estimated $d(X) \le 1 + \mathrm{const}\,\nu^{9/40}\tilde{L}^{3/2}$ (see ref. [133] and references therein), it is generally believed that in an extended system the fractal dimension grows linearly with the system size [217, 243, 75]. In practice, people tend to use much fewer modes to do the simulation than given by the above estimate. When restricted to the inertial manifold, the flow of the KSe is equivalent to that of a finite set of ODEs. In this sense, the KSe is accessible by the "low-dimensional" dynamical system analysis. In practice, we get the set of ODEs that define the dynamics on the inertial manifold by substitute the approximate constraint equations into the equations of motion of lower Fourier modes [250].

5.3 Steady solutions of the KSe

Though the KS equation is a nonlinear PDE and exhibits spatiotemporally chaotic behavior when the system size is big enough, it shows characteristics of low-dimensional dynamics, which is analytically justified by the study of inertial manifolds. From the trivial state $u \equiv 0$ towards the onset of the chaotic behavior, the system experiences a series of bifurcations in which steady solutions play an important role and set up the scale of the building blocks of spatiotemporal chaos. In certain parameter range, the steady solutions are directly related to the observed dynamics. For example, the n-cell state [92] is stable at discrete windows for arbitrary large system size. Another example is the localized near-solitory waves observed in experiments and numerical simulation [34]. These highly-separated waves are not stable and their evolution is governed by the weak interaction originating from the exponential tails of their profiles.

Equilibria are the simplest invariant sets in the phase space, their distribution and the connections between them form the coarsest geometrical frame for organizing phase space orbits [104]. The steady solutions of the KSe satisfies

$$(u^2)_x - u_{xx} - \nu u_{xxxx} = 0\,.$$

We can integrate once to get

$$u^2 - u_x - \nu u_{xxx} = c\,, \tag{138}$$

where c is an integration constant. Its value determines the property of solutions of (138). In the following calculation, without loss of generality we may set $\nu = 1$.

Written in the form of a $3-d$ dynamical system, (138) becomes

$$\begin{aligned} u_x &= y \\ y_x &= w \\ w_x &= u^2 - y - c\,. \end{aligned} \tag{139}$$

It is clear that the flow defined by (139) is volume preserving. Notice that the system has the time reversal symmetry,

$$x \to -x, \quad u \to -u, \quad y \to y, \quad w \to -w\,.$$

From (139), we see that

$$(u+w)_x = u^2 - c\,.$$

Therefore, if $c<0$, $u+w$ increases without bounded with $x \to \infty$. Every solution escapes to infinity and (139) has no bounded solutions. If $c=0$, the origin $(0,0,0)$ is the only bounded solution. Other solutions go to infinity when $x \to \infty$ and/or $x \to -\infty$. If $c>0$, interesting dynamics may happen and depending on the value of c, the set of bounded solutions can be extremely complicated. In the following, we only discuss this case. Again, the dynamics of (139) is organized at the coarsest level by its own equilibria and possible connections between them.

When $c>0$, system (139) has two stationary points $c_+ = (\sqrt{c},0,0)$ and $c_- = (-\sqrt{c},0,0)$. Linearizing the flow around c_+, we obtain the stability eigenvalues $2\lambda_1\,, -\lambda_1 \pm i\lambda_2$ with

$$\lambda_1 = \frac{1}{\sqrt{3}}\sinh\phi,\ \ \lambda_2 = \cosh\phi\,,$$

where $\sinh 3\phi = 3\sqrt{3c}$. So, c_+ has a $1-d$ unstable manifold and a $2-d$ stable manifold along which solutions spiral in. Because of the time reversal symmetry, c_- has similar manifolds with reversed stability properties. The escaping orbits still dominate and it can be shown that the escaping orbits take up a large subset in the phase space [23]. This creates great trouble for numerical calculation as most of the orbit will escape even near a compact invariant set. Bisection technique is used by the early authors [129] and evolves into straddle-saddle scheme later on [198, 188]. All these methods involve the time and effort consuming evolving-refining procedures. To efficiently locate important compact solutions, the variational technique developed in [158] shows its strength as we will show later.

5.3.1 Heteroclinic and homoclinic Connections

It is well known that equation (138) has an exact heteroclinic solution

$$u = a_1 \tanh(kx) + a_2 \tanh^3(kx)\,, \tag{140}$$

for the specific value $c = -\frac{30k^2}{19}(304k^4 - 40k^2 + 1)$ where

$$a_1 = 60k^3 - \frac{30k}{19}\,,\ a_2 = -60k^3\,,\ k^2 = \frac{11}{76} \text{ or } k^2 = -\frac{1}{76}\,.$$

When $k^2 = -1/76$, the hyperbolic tangent becomes ordinary tangent and there are poles on the real axis. Near the singulariy, u goes like like

$$u(x) \approx \frac{-60}{(x-x_0)^3}\,,\ x \to x_0\,.$$

All the blow-up solutions possess singularities of the same type [23]. In general, the existence and structure of connections depend on parameter c in a very complicated way.

According to the stability analysis of the stationary points of (139), naive counting scheme [263] tells that: there are structurally stable spiraling heteroclinic connections between c_+ and c_- for any $c > 0$. Connections may exist connecting the $1-d$ and the $2-d$ manifolds for discrete values of c. Due to time reversal symmetry, the two $1-d$ manifolds are sometimes able to connect to each other to form asymptotically monotonic connection. The exact solution (140) is an example.

When c is large, system behavior is quite simple. Let's do the following rescaling of coordinates

$$u \to \sqrt{c}u\,,\ x \to \frac{x}{c^{1/6}}\,.$$

(138) then becomes

$$u^2 - c^{-1/3}u - u_{xxx} = 1\,.$$

In the limit $c \to \infty$, we get

$$u_{xxx} = u^2 - 1\,.$$

McCord studied this system and proved that the antisymmetric heteroclinic orbit connecting the two equiliria is the only bounded nonconstant solution [175]. For c large enough, Michelson argued that the heteroclinic orbit remains the unique bounded curve [177]. This orbit has been numerically observed down to $c = 0.07$ [129] and can be found in normal form analysis for $c \ll 1$ [33].

When c decreases from large values, new connections with more zeroes are born through saddle-node bifurcations. They all lie on the 2-d manifolds of $c_\pm$ and so possess structural stablility. There exists a lower bound $c_{max} \approx 1.1252$ such that these orbits limit to an odd periodic orbit by having infinitely many zeroes at $c = c_{max}$. When $c < c_{max}$, the set of connections has intricate geometrical structure. Lau [161] has studied the formation and bifurcation of the intersectons of 2-d manifolds of $c_\pm$ and found that they form a cocoon-like tangle in the phase space. He named the whole process the "cocoon" bifurcation.

In [129], if a heteroclinic orbit involves spiraling, it is called an oscillatory shock, otherwise, a regular shock. Homoclinic connections are called solitory waves. More specifically, in the far field, the oscillatory shock behaves like

$$u \to \pm\sqrt{c} + b_\pm e^{\mp\lambda_1 x}\cos(\lambda_2 x + \phi_\pm)\,,\ x \to \pm\infty\,, \tag{141}$$

the regular shock behaves like

$$u \to \mp\sqrt{c} + a_\pm e^{\mp 2\lambda_1 x}\,,\ x \to \pm\infty\,, \tag{142}$$

and the solitary wave near c_+ behaves like

$$\begin{aligned} u &\to \sqrt{c} + a e^{2\lambda_1 x}\,, && x \to -\infty \\ u &\to \sqrt{c} + b e^{-\lambda_1 x}\cos(\lambda_2 x + \phi)\,, && x \to +\infty\,, \end{aligned} \tag{143}$$

where $a, a_\pm, b, b_\pm$ are arbitrary constants and $\phi, \phi_\pm$ are adjustable parameters to match asymptotics when $x \to \pm\infty$. The three categories are investigated numerically at different c values in [129] and families of solutions are found. These connecting orbits can be classified according to their topology relative to the two equilibria [145].

The asymptotic approach can sometimes be rather tricky. For example, when $c \to 0^+$, although an asymptotic expansion appears to establish the existence of regular shocks, there are actually none. Only the "asymptotics beyond all orders" reveals the truth [106]. Yang carried out the asymptotic analysis further on the existence and properties of the connections [279]. He showed that in the weak-shock limit, *i.e.*, $0 < c \ll 1$, the oscillatory shocks can only be antisymmetric, otherwise oscillatory and monotonic waves of exponentially small but growing amplitude will be excited. He also showed that under certain conditions, the solitary wave forms when the stable and unstable manifold of an equilibrium connects.

Numerically, the asymptotic solutions are taken as the initial condition and shooting scheme is invoked to determine the connections. The integration constant c and the azimuthal angle ϕ can be used as variable matching parameters. There are two ways of shooting. The first is to shoot from one point and check whether it reaches the other point; the other is to shoot from both points and match them at some intermediate point. I prefer the second method as matching away from the equilibria is easier and more accurate.

5.3.2 Periodic Solutions of the steady equation

Having in mind above discussion about the intricate set of connections, we expect that the set of periodic solutions could be extremely complicated. Yet a bifurcation analysis in Fourier space simplifies the classification a lot if we are only concerned with the periodic solutions [104]. For a fixed system size L, the periodic solutions satisfy the equation

$$[(kq)^2 - (kq)^4]a_k + ikq\sum_{m=-\infty}^{\infty} a_{k-m}a_m = 0\,. \tag{144}$$

We have proved in sect. 5.2.2 that when the system size is smaller than 2π, the laminar state $u \equiv 0$ is the global attractor. So there is no nontrivial periodic solution with period smaller than 2π. Next we check the linear stability of the laminar state. When the nonlinear term $(u^2)_x$ is removed in (133), the remaining linear equation has Fourier modes as eigenvectors with eigenvalues

$$\omega_k = (kq)^2 - (kq)^4 \,.$$

If we take the system size L as the bifurcation parameter, every time L crosses $2n\pi \,, n \in \mathbb{N}$, there is a pitchfork bifurcation where n-cell states are generated. They form an invariant circle due to the translational invariance of (133). In the antisymmetric space, they corresponds to two points, being half-period translates of each other, and of the form

$$u(x,t) = -2 \sum_k b_{kn} \sin(knx) \,,$$

where $b_{kn} \in \mathbb{R}$. By rescaling u, x and ν, the n-cell states transform to each other.

The bifurcation of the n-cell states is well described in [104]. The stability matrices associated with these states decompose into non-interacting blocks due to the symmetries present. Each block corresponds to a subharmonic perturbation and contains two separate subsectors corresponding to cosine and sine components in the tangent space. At each bifurcation, two anti-symmetric solutions (being translates of each other) are generated with additional asymmetric solutions. For small long-wavelength perturbations, the anti-symmetric solution can be viewed as a modulated n-cell state.

With the increase of L these steady periodic solutions may bifurcate into more complicated ones. For any fixed period L, however, the number of steady periodic solutions are finite up to spatial translation. This fact can be explained as follows. The existence of the inertial manifold [249] bounds the size of all Fourier components and the stationary points should live on the compact inertial manifold. This manifold and the dynamics on it can be described by smooth functions of a finite number of Fourier modes. On a finite-dimensional compact manifold, a smooth function can only have a finite number of zeros. So, the steady states, as the zeros of the smooth velocity field on the inertial manifold, are finitely many.

When L is small, the number of steady solutions are small and their energy concentrates on the low wavenumber end of the Fourier spectrum. These solutions may be obtained by solving the truncated version of (144). When L increases, the number of steady solutions increases exponentially. Like the laminar solution, a steady solution bifurcates every time when L expands a certain amount close to some average value. In the limit of infinite system size $L \to \infty$, there are infinitely many steady solutions. To understand the structure of these solutions, we have to study the phase space of the $3-d$ dynamical system (139).

The mass generation of periodic orbits are closely related to the connecting orbits in the phase space. Kent and Elgin conjectured that all the bounded orbits originate from the unique heteroclinic orbits at $c \gg 1$ through a series of bifurcations [145]. The existence of the periodic and connecting orbits may be rigorously established by computer-assisted topological arguments [255]. At the qualitative level, the existence of the complicated set of periodic orbits is deducible from the Shil'nikov construction of horseshoes for homoclinic orbits or heteroclinic cycles [107]. There are infinitely many horseshoes associated with this construction and each horseshoe will generate infinitely many periodic orbits. So, the orbit structure of the phase space becomes extemely complicated when this construction is possible. But there is no problem for the periodic orbit theory as periods of these orbits

increase very fast and the required low-period orbits can be found numerically without much difficulty.

5.3.3 Phase space structure at small c

In the limit $c \to 0^+$, perturbation technique can be employed to analyze properties of (139). For simplicity, let $c = \epsilon^2 \,,\ \epsilon > 0$. Make a change of variables

$$(u, y, w) \to \epsilon(u, y, w) \,.$$

(139) becomes

$$\begin{aligned} u_x &= y \\ y_x &= w \\ w_x &= -y + \epsilon(u^2 - 1) \,. \end{aligned} \tag{145}$$

To the zeroth order, (145) is linear, the general solutions is

$$\begin{aligned} u &= \tilde{y}\sin(x) - \tilde{w}\cos(x) + \tilde{u} \\ y &= \tilde{y}\cos(x) + \tilde{w}\sin(x) \\ w &= -\tilde{y}\sin(x) + \tilde{w}\cos(x) \,, \end{aligned} \tag{146}$$

where $\tilde{u}, \tilde{y}, \tilde{w}$ are constants and will be used as dependent variables in the perturbation analysis. Substitute (146) into (145), and we get equations for $\tilde{u}, \tilde{y}, \tilde{w}$,

$$\begin{aligned} \tilde{u}_x &= \epsilon(u^2 - 1) \\ \tilde{y}_x &= -\epsilon\sin(x)(u^2 - 1) \\ \tilde{w}_x &= \epsilon\cos(x)(u^2 - 1) \end{aligned} \tag{147}$$

Multi-scale averaging method may be used to analyze (147). For example, do the following change of variables,

$$\tilde{y} = \bar{y} + \epsilon y_1(\bar{u}, \bar{y}, \bar{w}, x) + \epsilon^2 y_2(\bar{u}, \bar{y}, \bar{w}, x) + \cdots \,,$$

with similar expressions applied to the other two variables, $\tilde{u}$ and $\tilde{w}$. To the third order of ϵ, we get (for notation simplicity we replace $\bar{u}, \bar{y}, \bar{w}$ by u, y, w)

$$\begin{aligned} u_x &= \epsilon[\frac{1}{2}(y^2 + w^2) + u^2 - 1] + \epsilon^3[4u^4 + \frac{7}{4}(y^2 + w^2) - \frac{271}{288}(y^2 + w^2)^2 \\ &\quad + \frac{1}{8}u^2(-32 + 9(y^2 + w^2))] \\ y_x &= -\epsilon uy + \frac{\epsilon^2}{24}(36u^2 w - w^3 - wy^2) + \frac{\epsilon^3}{36}[153u^3 y - 9uy - 41uy(y^2 + w^2)] \\ w_x &= -\epsilon uw - \frac{\epsilon^2}{24}(36u^2 y - y^3 - yw^2) + \frac{\epsilon^3}{36}[153u^3 w - 9uw - 41uw(y^2 + w^2)] \,. \end{aligned}$$

Let $\rho = y^2 + w^2$, we get a 2-d dynamical system

$$\begin{aligned} u_x &= \epsilon(\frac{1}{2}\rho + u^2 - 1) + \epsilon^3(4u^4 + \frac{7}{4}\rho - \frac{271}{288}\rho^2 + \frac{1}{8}u^2(-32 + 9\rho)) \\ \rho_x &= \epsilon 2u\rho + \frac{\epsilon^3}{18}(153u^3\rho - 9u\rho - 41u\rho^2) \,. \end{aligned} \tag{148}$$

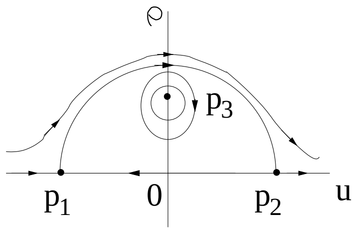

Figure 14: Phase diagram of (148) to the lowest order.

This is a 2-d autonomous system with $(x-)$time reversal symmetry, *i.e.*, the system is invariant under

$$u \to -u\,, \rho \to \rho\,, x \to -x\,.$$

H.-T. Chang obtained a similar expression to the lowest order of ϵ using the normal form analysis [33]. To $O(\epsilon^2)$, the phase diagram of system (148) is shown in figure 14. There are three stationary points $p_1\,, p_2\,, p_3$ where p_1 and p_2 correspond to the two stationary points of (139) and p_3 to the odd periodic orbit generated when c crosses zero. As shown in [141], this orbit always exists for small $c > 0$ and has the form

$$u = -\sqrt{2}\epsilon\sin(\Omega x) + \frac{\epsilon^2}{3}\sin(2\Omega x) + \cdots\,,$$

where $\Omega = 1 - \epsilon^2/6 + \cdots$. The existence of this orbit and the structurally stable heteroclinic connection implies an extremely complicated phase space structure as consequence of the Conley index theory [43] and Shil'nikov construction [107]. In figure 14, we have two heteroclinic connections between p_1 and p_2. The one on the $\rho = 0$ axis corresponds to the regular shock mentioned before and the other one to a 2-d connection manifold of (139). Between these connections, the area is filled with periodic orbits, corresponding to invariant tori of (139), whose periods increase indefinitely upon approaching the connections.

The dynamics described above is not structurally stable. It depicts, however, a qualitative picture valid to all orders of ϵ, which seems to say that through change of coordinates, the system (139) becomes an integrable system. This *cannot* be correct as complicated dynamical behavior is observed in (139) even for small values of c. The contradiction is due to the nonconvergence of the series of coordinate changes

$$\tilde{y} \to \bar{y} + \epsilon y_1 + \epsilon^2 y_2 + \cdots\,.$$

For this reason, many features of the dynamics observed in figure 14 are not present in (139). For example, there are no continuous families of invariant tori or 2-d heteroclinic connection, and the connection on $\rho = 0$ does not exist for small $c > 0$, as noted above. In fact the separation of the $1-d$ manifolds can be estimated using the analysis beyond all orders [106]. Similar situations are frequently encountered in Hamiltonian mechanics [126, 152]. On the other hand, many features of (148) are kept in (139). For example, some of the invariant tori would survive the higher order perturbations [189] and one structurally stable heteroclinic connection persists as a remnant of the $2-d$ connection manifold. During the process, infinitely many periodic orbits will be generated.

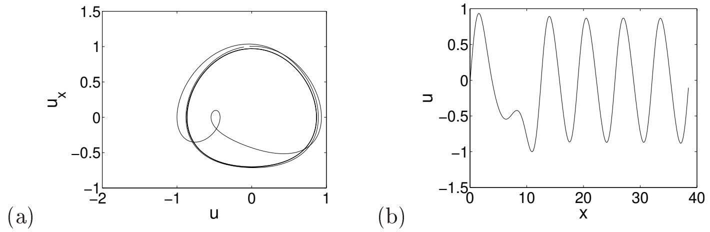

Figure 15: A non-symmetric steady solutions of (135),$L = 38.5\,, \nu = 1$. (a) u, u_x projection in the 3-d phase space of (139); (b) The profile of the same orbit on the interval $[0, L]$;

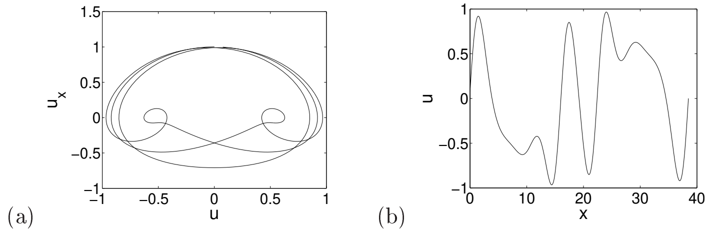

Figure 16: The first antisymmetric steady solutions of (135),$L = 38.5\,, \nu = 1$. (a) u, u_x projection in the 3-d phase space of (139); (b) The profile of the same orbit on the interval $[0, L]$;

5.3.4 Variational approach

Because we take the periodic boundary conditions $u(x, t) = u(x + L, t)$, it is of great interest to find dynamically important steady solutions with a given spatial period L. (144) may be directly solved for the steady solution. But as we remarked previously, the number of solutions increases rapidly with L, if L is not too small, there are quite many low-period orbits and we have to classify them according to their importance as we believe that only a few of them are closely related to the asymptotic dynamics of (133). Empirically, we know that an equilibrium is important if a typical phase orbit passes its neighborhood frequently. On a plane, through observation of phase orbits we may quickly identify those important equilibria. In high dimensional space, even if the steady solutions are found, it is not straightforward to determine which ones are important.

We pick up any point on a typical orbit of (135). It corresponds to an antisymmetric loop in the phase space $\mathcal{M}$ of (139) and so can be used to initialize the search for a periodic orbit in $\mathcal{M}$. Using the technique developed in [158], we found several dozen periodic orbits of (139) for $L = 38.5\,, \nu = 1$. Not all of them are antisymmetric and some of them may not even be important. We show a non-symmetric orbit in figure 15. It is not in the antisymmetric solution space of the KSe. Next we re-initialize the search by taking the average of an orbit segment of (135) with the hope that the typical phase orbit will pass through the neighborhood of important steady solutions often. In this way, the number of relevant steady solutions is greatly reduced. There are around 10 solutions with 5 of them antisymmetric. We display them in figure 16, figure 17, figure 18, figure 19, and figure 20.

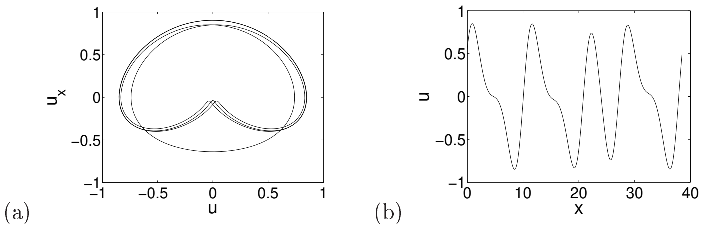

Figure 17: The second antisymmetric steady solutions of (135),$L = 38.5\,, \nu = 1\,.$ (a) u, u_x projection in the 3-d phase space of (139); (b) The profile of the same orbit on the interval $[0, L]$;

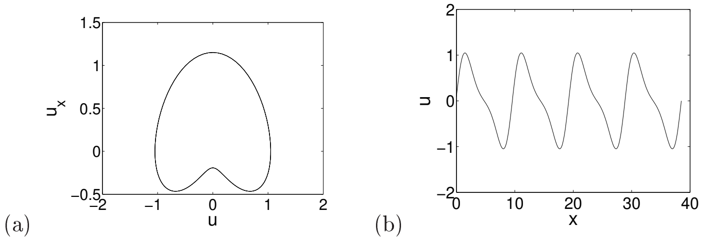

Figure 18: The third antisymmetric steady solution of (135),$L = 38.5\,, \nu = 1\,.$ (a) u, u_x projection in the 3-d phase space of (139); (b) The profile of the same orbit on the interval $[0, L]$;

Close inspection reveals that the steady solutions have different topology relative to the equilibria on the u, u_x projection plane of $\mathcal{M}$. In figure 17 and figure 18, the orbits circle the pair of stationary points as a whole and u has 4 peaks on $[0, L]$. In figure 15, figure 16, figure 19, figure 20, the orbits circle both the pair and the individual equilibria. As we may notice, all the solutions have different circulations so the circulation around the two equilibira may be used to classify the steady solutions as mentioned earlier. Each circulation gives a peak in the u profile on $[0, L]$ with big circulations giving large main peaks and small ones giving secondary ripples. The profiles in figure 15, figure 19, figure 20 has 6 peaks while there are 5 peaks in figure 16.

5.3.5 Other bounded solutions

Besides stationary points, heteroclinic connections and periodic orbits, there are other more complicated invariant sets like invariant tori and chaotic trajectories. Interestingly, almost all these solutions exhibit the characteristic cellular structure - the average distances between maxima or minima approximately equal a constant value close to $2\sqrt{2}\pi$, the wavelength of the most unstable mode.

The periodic orbits can be either elliptic or hyperbolic. When they are elliptic, the Poincaré map associated with the periodic orbit is measure preserving and Moser's twist mapping theorem implies that, the flow defined by (139) possesses an infinite set of invariant tori surrounding the periodic orbit [177]. When a periodic orbit is hyperbolic, there exists

Kuramoto-
Sivashinsky
system—)

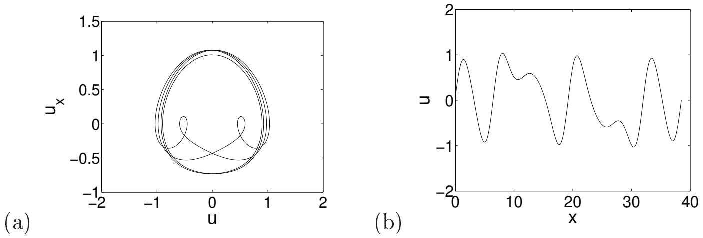

Figure 19: The fourth antisymmetric steady solution of (135),$L = 38.5\,, \nu = 1\,.$ (a) u, u_x projection in the 3-d phase space of (139); (b) The profile of the same orbit on the interval $[0, L]$;

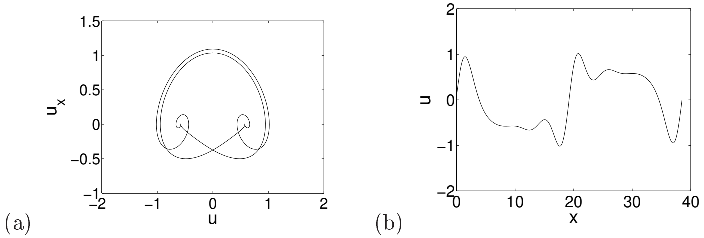

Figure 20: The fifth antisymmetric steady solutions of (135),$L = 38.5\,, \nu = 1\,.$ (a) u, u_x projection in the 3-d phase space of (139); (b) The profile of the same orbit on the interval $[0, L]$;

Cantor-type set of chaotic solutions which weave between periodic ones. This can be double-checked by constructing horseshoes from the connections.

5.4 Summary

In this chapter, we derived the KSe as a phase equation from the CGLe. Eq (133) is a general phase equation in a space-time translationally invariant system when the system crosses the long wavelength instability [154]. We discussed its basic property, in particular, its inertial manifold. We also gave a detailed account of its steady solutions. It turns out that even the structure of the set of steady solutions is rather complex. Lots of efforts have been invested to illucidate the spatial behavior of these solutions.

Steady solutions are important because they set up the coarsest frame for the typical phase space motion. According to their distribution and property, the phase space is divided into qualitatively different parts. Each part has its own dynamics and there are orbits commuting between different parts. In the next chapter, we will investigate all these dynamics in detail and build a much more clear picture of the SIS.